LLNL-JRNL-818633

LAWRENCE
LIVERMORE
NATIONAL
LABORATORY

A variance-based decomposition and global sensitivity index method for uncertainty quantification: Application to retrieved ice cloud properties

X. Chen, Q. Tang, S. Xie, C. Zhao

January 22, 2021

Journal of Geophysical Research: Atmospheres

A Variance-Based Decomposition and Global Sensitivity Index Method for Uncertainty Quantification: Application to Retrieved Ice Cloud Properties

Xiao Chen,[1] Qi Tang,[2] Shaocheng Xie[2] and Chuanfeng Zhao[3]

Corresponding author: X. Chen, Center for Applied Scientific Computing, Lawrence Livermore National Laboratory, 7000 East Ave., Livermore, CA 94550, USA. (chen73@llnl.gov)

[1]Center for Applied Scientific Computing,
Lawrence Livermore National Laboratory,
Livermore, California, USA.

[2]AEED-Atmospheric, Earth and Energy,
Lawrence Livermore National Laboratory,
Livermore, California, USA.

[3]College of Global Change and Earth
System Science, Beijing Normal University,
Beijing, China.

Abstract.

This study develops a novel uncertainty quantification (UQ) method for cloud microphysical property retrievals using variance-based decomposition and global sensitivity index. In this UQ framework, empirical orthogonal function (EOF) analysis is applied to the U.S. Department of Energy Atmospheric Radiation Measurement (ARM) ground-based observations, which are the inputs for the cloud retrieval studied here. The principal components (PCs) in the EOF expansion are parameterized as random input variables, and hence the input dimension is greatly reduced (up to a factor of 50), allowing large ensemble of random samplings. The EOF expansion improves the accuracy of the uncertainty estimation by taking into account the cross correlations in the input data profiles. This method enables a probabilistic representation of a retrieval process by adding normally distributed perturbations into PCs of sample-means of input data profiles within a time window. Therefore, it effectively facilitates objective validation of climate models against cloud retrievals under a probabilistic framework for rigorous statistical inferences. Moreover, the variance-based global sensitivity index analysis, part of this method, attributes the output uncertainties to each individual source, thus providing directions for improving retrieval algorithms and observation strategies. For demonstration, we apply this method to quantify the uncertainties of the ARM program's baseline cloud retrieval algorithm for an ice cloud case observed at the Southern Great Plains site on March 9, 2000.

1. Introduction

Cloud microphysical properties such as liquid and ice water contents retrieved from ground-based measurements are important geophysical quantities that are often used in developing and evaluating cloud parameterizations in climate models. However, studies have shown that large differences and uncertainties exist in ground-based cloud retrievals [*Comstock et al.*, 2007; *Turner et al.*, 2007; *Zhao et al.*, 2012; *Huang et al.*, 2012]. The retrieval uncertainties are primarily caused by uncertainties in the retrieval theoretical bases, assumptions, input data, and constraint parameters as indicated in these studies. Quantitative knowledge about the retrieval uncertainties has thus been long desired by the climate modeling community to better constrain model-produced cloud properties [*Xie et al.*, 2005; *Xu et al.*, 2005; *Xie et al.*, 2011].

A traditional way to estimate uncertainty is to randomly perturb input data profiles and several key retrieval parameters used in a single cloud retrieval technique. The standard deviation from the ensemble mean of the perturbed retrieval is considered as a proxy of the uncertainty [*Zhao et al.*, 2014]. The other way to estimate uncertainty is to calculate the mean and standard deviation from multiple unperturbed cloud retrievals based on different retrieval techniques and ground-based remote sensors [*Comstock et al.*, 2007]. In recent years, several studies estimate retrieval uncertainties through a radiative transfer model and apply Bayesian calibration to statistically compare the surface and top-of-atmosphere (TOA) radiative fluxes and other properties to observations [*Posselt et al.*, 2008; *Comstock et al.*, 2013]. One can further apply multi-model Bayesian model selection, and model discrepancy techniques to mitigate the uncertainty estimated by multi-retrieval algorithm [*Määttä et al.*, 2014].

The above methods suffer from but are not restricted to the following limitations: (1) the cross correlations in the input data profiles are often not considered; (2) parameterizing input data profiles with appropriate cross correlations is not an obvious task; (3) sampling random variables amongst vertical layers, which could be on the order of hundreds depending on the vertical resolution, requires an enormous, infeasible sampling size; (4) characterizing probability density functions (PDFs) of the random variables often require unrealistic statistical hypotheses; (5) attributing the variability in the retrieval output to that in each individual uncertainty source (i.e., global sensitivity analysis) is not permitted in general; and (6) differences between measurements and the truth (i.e., bias analysis) are usually not considered.

To address these issues, we propose an uncertainty quantification (UQ) and sensitivity analysis methodology based on Karhunen-Loéve expansion (KLE), Central-Limit Theorem (CLT), and Sobol' indices. The KLE [*Kuhunen*, 1947; *Loéve*, 1945] is a principal component analysis (PCA) [Wilks, 2011], which transforms a number of possibly correlated variables into a smaller number of uncorrelated variables called principal components (PCs) through the empirical orthogonal function (EOF) expansion. For the first issue, the application of the EOF expansion to ground-based cloud measurements such as those from the U.S. Department of Energy (DOE) Atmospheric Radiation Measurement (ARM) program allows us to obtain the cross correlations of input data profiles within a given time window. In this study, we use a 0.5-hour time window, comparable to the typical climate model temporal resolution.

For the second issue, a stochastic representation of input data profiles is constructed by using the PCs of the EOF expansion as input random variables, associated with the extracted observational covariance matrix within the 0.5-hour time window. Hence the uncertainty is automatically embedded in the EOF expansion by adding appropriate perturbations into the PCs. Since random perturbations are added into the PCs instead of into each vertical layer of the input data profiles, the dimensionality of the stochastic space (issue (3)) is significantly reduced so that it reduces the sampling size required to stabilize the statistics of the cloud retrieval.

Since the target of this study is the 0.5-hour sample-mean of the stochastic data profile, the CLT [*Cramér*, 1946; *Gnedenko et al.*, 1954; *Storch and Zwiers*, 2002] can be leveraged to solve the issue (4). Based on the CLT, the normally distributed perturbations are thus added on the extracted input random variables (proof is provided in Appendices A and B). To address the issue (5), we apply the variance-based global sensitivity index analysis [*Sobol*, 1993] to the retrieval algorithm and attribute the uncertainties of vertically resolved retrieval output to the input random variables as well as retrieval parameters. These sensitivity indices can provide insights for improving retrieval algorithms and observation strategies.

In summary, we employ the probabilistic PCA to enable the stochastic cloud retrieval by adding observation-based perturbations to the PCs of the EOF expansion of the sample-mean of input data profiles following normal distributions per CLT. The variance-based sensitivity analysis attributes the vertically resolved retrieval output uncertainties to each individual source. This variance-based UQ method effectively facilitates objective validation of climate models against cloud retrievals under a probabilistic framework for rigorous statistical inferences. It should be noted that the retrieval model structural uncertainty and the bias are not addressed in the current work.

The structure of the paper is as follows. In Section 2, details of the probabilistic PCA based uncertainty analysis in cloud microphysical property retrievals are given. In Section 3, the capability of the UQ method is illustrated with an ice cloud case using the ARM baseline cloud microphysical algorithm (MICROBASE). Results from our uncertainty analysis and sensitivity study are shown in Section 4, followed by conclusions and discussions in Section 5.

2. Methodology

The EOF analysis is a variance-based statistical technique designed for decomposition of time series in terms of orthogonal basis functions that are determined from the empirical data. The orthogonal basis functions are chosen to account for as much as variance of the empirical data as possible. In this paper, the EOF analysis is applied to the ARM measurements required as the MICROBASE inputs with 0.5-hour interval. The realizations of the random variables in the EOF expansion are computed by projecting empirical ARM measurements on the orthogonal basis functions. In general, the probabilistic distributions of the random variables cannot be determined by these realizations. According to the CLT, however, the sample-means of these random variables are normally distributed when the number of measurements is large enough (a sampling size greater than 30 is generally considered as large enough) within the time window. Therefore, it enables the probabilistic representation of a stochastic retrieval process by adding normally distributed perturbations to the PCs of the EOF representation of the sample-means of the input data profiles (see Appendix B).

To demonstrate the probabilistic PCA based method, we start with a temporal-spatial stochastic process denoted as $Y(\mathbf{x}, t, \theta)$ to represent stochastic input data profiles for the retrieval algorithm, where $\mathbf{x}$ denotes the height, t the time, and θ a random event. For example, $Y(\mathbf{x}, t, \theta)$ can be referred as the radar reflectivity profile that will be described in Section 3. Accordingly, an ensemble of snapshots of the stochastic process $Y(\mathbf{x}, t, \theta)$ observed in the time window $[0, T]$ can be recorded as

$$\{y_1, y_2, \ldots, y_n\}, \tag{1}$$

where $y_i(\mathbf{x}) = y(\mathbf{x}, t_i)$, $i = 1, \ldots, n$, n is the number of snapshots; and the ensemble average of the snapshots can be defined as $\bar{y}(\mathbf{x}) = \frac{1}{n}\sum_{i=1}^{n} y_i$.

With measurement noises added to the stochastic process $Y(\mathbf{x}, t, \theta)$, we have a perturbed input data profile denoted as $Y'(\mathbf{x}, t, \theta)$ and it can be written as

$$Y'(\mathbf{x}, t, \theta) = Y(\mathbf{x}, t, \theta) + \text{noise}. \tag{2}$$

The stochastic process $Y(\mathbf{x}, t, \theta)$ can be decomposed into the ensemble average $\bar{y}(\mathbf{x})$, and an intrinsic unknown random estimation error $\epsilon(\mathbf{x}, t, \theta)$, such that

$$Y(\mathbf{x}, t, \theta) = \bar{y}(\mathbf{x}) + \epsilon(\mathbf{x}, t, \theta). \tag{3}$$

Therefore, the perturbed stochastic process $Y'(\mathbf{x}, t, \theta)$ can be decomposed as

$$Y'(\mathbf{x}, t, \theta)) = \bar{y}(\mathbf{x}) + \epsilon(\mathbf{x}, t, \theta) + \text{noise}. \tag{4}$$

One goal of this paper is to quantify the cloud retrieval uncertainties for climate model evaluation. The typical climate model temporal resolution is currently

Thus, the perturbed input data profile $Y'(\mathbf{x}, t, \theta)$ is transformed to a smoother statistic $\overline{Y'}(\mathbf{x}, t, \theta)$, which is the sample-mean of $Y'(\mathbf{x}, t, \theta)$ within the 0.5-hour time window. Given a time window, the statistic $\overline{Y'}(\mathbf{x}, t, \theta)$ is also a random variable and it approximately follows a normal distribution when the sampling size within the time window is large enough (large number law) [*Storch and Zwiers*, 2002].

Due to the high dimensionality of the stochastic space for $Y'(\mathbf{x}, t, \theta)$ (e.g., 512 vertical layers in the ARM radar reflectivity profiles), it is computationally infeasible to sample all the vertical layers individually. To reduce the dimensionality, we apply the EOF expansion to represent the perturbed stochastic process $Y'(\mathbf{x}, t, \theta)$ in terms of eigenfunctions of its correlation kernel assuming that it is piece-wise constant within the 0.5-hour time window. The detailed derivations can be found in Appendices A and B.

By applying the CLT to the ARM ground-based observations, in Appendix B we show that random variables appeared in the EOF expansion of $\overline{Y'}(\mathbf{x}, t, \theta)$ approximately follow normal distribution when the sampling size is large enough. By truncating EOF expansion of $\overline{Y'}(\mathbf{x}, t, \theta)$ to the order of M, we finally arrive at $\overline{Y'}(\mathbf{x}, t, \theta)$ that is the sample-mean of the perturbed data profile with white noises added and it can be written explicitly as

$$\overline{Y'}(\mathbf{x}, t, \theta) = \bar{y} + \sum_{i=1}^{M} \psi_i \sqrt{\frac{\lambda_i}{n}} \sqrt{1 + \left(\frac{\sigma_0}{\sqrt{\frac{\lambda_i}{n}}} \right)^2} \frac{z_i}{\sqrt{n}} + error(\mathbf{x}, t, \theta), \tag{5}$$

where $z = [z_1, z_2, \ldots, z_M]^{\mathbf{T}}$ follows a standard multivariate normal distribution, i.e., $z \sim \mathcal{N}(0, \mathbf{I}_M)$ and $\mathbf{I}_M$ is a $M \times M$ identity matrix; (λ_i, ψ_i) are corresponding pairs of eigenvalues and eigenfunctions; σ_0 denotes the standard deviation of normally distributed random measurement noises; $error(\mathbf{x}, t, \theta)$ is the truncation error. The detailed proof is given in the Appendix B. To simplify, other than observation-based input data profiles, uniform distributions are applied to perturb the retrieval parameters.

We apply Sobol's method to derive the global sensitivity analysis of microphysical properties retrieved by MICROBASE. Sobol's method is a variance-based sensitivity analysis method, which divides the variance $\mathrm{Var}\left(\overline{Y'}\right)$ into fractions attributed to each input X_i (first-order sensitivity or main effect indices $S_i = \dfrac{V_i}{\mathrm{Var}\left(\overline{Y'}\right)}$ where $V_i = \mathrm{Var}_{X_i}\left(E_{X\sim i}\left(\overline{Y'} \mid X_i\right)\right)$ defined as average over variations in other random inputs or parameters), and their interactions (second-order sensitivity indices S_{ij} or higher-order indices formed by dividing other terms in the variance decomposition). The fractions measure the contribution to the output variances of each input variable, including all interactional variances with any other input variables in all the orders. The sum of all the Sobol's indices equals to one. Also, Latin Hypercube Sampling (LHS) procedure is used to draw samples in the designed space for the input random variables and retrieval parameters. LHS is an effective stratified sampling approach in a high-dimensional space ensuring that all portions (with equal probability) of a given partition are sampled [*McKay et al.*, 1979].

3. Case Study

For demonstration, we apply the probabilistic PCA to propagate uncertainties from ARM ground-based measurements as well as empirical parameters used in MICROBASE into its retrieved products for uncertainty quantification and analysis. MICROBASE is the ARM base-line cloud microphysical property retrieval algorithm based on the cloud radar and lidar measurements [*Dunn et al.*, 2011; *Zhao et al.*, 2014]. It derives the cloud liquid and ice properties using empirical regression equations obtained from in situ aircraft measurements. Liquid water content (LWC) and ice water content (IWC) are derived from radar reflectivity measured by Millimeter Wavelength Cloud Radar (MMCR) with a frequency of 35 GHz. In MICROBASE, LWC is retrieved by

$$LWC = LWP \frac{Ze_{Liq}^{g}}{\sum_{i=1}^{n} Ze_{Liq}^{g} \Delta Z}, \tag{6}$$

whereas for pure ice clouds, IWC is retrieved by

$$IWC = aZe_{Ice}^{b}. \tag{7}$$

In the equations above, a, b and g are empirical parameters, and ΔZ is the vertical increment. LWP represents the liquid water path, while Ze_{Liq} and Ze_{Ice} represent the effective radar reflectivity profile for the liquid and ice, respectively. These Z-IWC empirical parameters in the retrieval algorithm are determined with certain assumptions about the ice particle size distribution, ice particle shape, and density [*Liu and Illingworth*, 2000]. Uncertainties in the retrieved quantities come from three sources: input profiles, the retrieval algorithms, and parameter assumptions as described in *Zhao et al.* [2012, 2014]. The uncertainty of input profiles is present in terms of two components, bias (related to accuracy measuring difference between measurements and truth), and the unavoidable random variations in measurements (related to precision). The bias of input data profiles and retrieval model structural uncertainty are not considered in this research article.

For the selected case study, we apply our probabilistic PCA based method to quantify uncertainties in MICROBASE retrieved ice for the high cirrus cloud case observed at the ARM SGP CF site on March 9, 2000 during the year 2000 cloud intensive observational period. This cirrus cloud case has been studied comprehensively by *Comstock et al.*

[2007] to examine ice cloud properties from 15 state-of-art cloud retrievals. As described by *Comstock et al.* [2007], the cirrus clouds were associated with the passage of a weak upper-level disturbance over the SGP region and deepened as the disturbance moved northeastward. Accordingly, optically thin ice clouds were observed initially (19:00–19:15 UTC) and between 22:00 and 22:30 UTC. The majority of the observed clouds were optically thick clouds over the 3.5-hour time period as shown in Fig. 1a. *Comstock et al.* [2007] shows large uncertainties in the retrieved ice cloud properties among the tested algorithms for both optically thin (optical depth, $\tau < 0.3$) and thick ($0.3 < \tau < 5.0$) cirrus clouds.

The detailed procedures of applying the probabilistic PCA based method to MICROBASE are described as the following. First, in order to efficiently represent uncertainty of input radar reflectivity profiles, we apply the PCA analysis to reduce the dimensions from 512 layers to 10 modes (the first four EOFs or modes of the PCA are shown in Fig. 2) to capture greater after 90% variance in the observed radar reflectivity profiles (Fig. 1a) and extract uncorrelated, independent random variables with orthogonal modes. For this test case, we assume that the correlation kernel of the stochastic radar reflectivity profile is piece-wise constant within each 0.5-hour time window. The details of computing eigenvalues and EOFs based on snapshots taken for an ensemble of relative errors can be found in Appendix A. As a result, we expand the input radar reflectivity profiles in terms of pairs of obtained eigenvalues and EOFs combined with associated PCs. The probabilistic distributions of these PCs in the EOF expansion of the stochastic input radar reflectivity profiles are generally unknown.

The stochastic radar reflectivity profile is transformed to a smoother statistic, which is the sample-mean of the observed ones within the 0.5-hour time window. Within each 0.5-hour time window, we have 180 times of observations (sampling size > 30). Based on the CLT, the sample-mean of the radar reflectivity profile is thus expanded in terms of independent and normally distributed random variables. The perturbation ranges of the input data and empirical parameters follow *Zhao et al.* [2014] and the cloud retrieval and measurement experts' suggestions (personal communications). The measurement noise of the radar reflectivity profile for each layer, denoted as σ_0, is chosen to be 1.0 dBZ. The range of the empirical parameter "a" is 0.03–0.22 $(\mathrm{g/m^3})$ /dBZ, while the empirical parameter "b" is assumed to be a dimensionless constant 0.59. The value 0.59 is chosen by the original MICROBASE algorithm for the parameter "b". We opt not to perturb the parameter "b", as the main purpose of this paper is to demonstrate the capacity of our UQ method instead of thoroughly exploring the uncertainties in the Z-IWC empirical relationship. Based on Eq. (5), the normally distributed perturbations are added on the independent random variables for the sample-mean of the radar reflectivity profile. Uniform distributions are assumed for the parameter "a".

We utilize the Problem Solving environment for Uncertainty Analysis and Design Exploration toolkit (PSUADE) [*Tong*, 2009] to perform the uncertainty and sensitivity analysis. PSUADE is a software toolkit for performing uncertainty analysis, responsive surface analysis, global sensitivity analysis, design optimization, model calibration, with large number of parameters and complex constraint. The samples of the random variables including PCs in the EOF expansion and empirical parameters in MICROBASE are obtained by uniform LH sampling using PSUADE. Based on Eq. (5), the PCs in the EOF expansion follow normal distributions. Therefore, the uniformly generated samples are thus converted to normally distributed ones for the PCs. Based on the uncertainty analysis performed by PSUADE, Figs. 1b and 1c compare the 0.5-hour averages of IWC from the original (unperturbed) MICROBASE and probabilistic PCA based ensemble means (ensemble size = 1000) of 0.5-hour sample-mean of IWC from the perturbed MICROBASE. Note that the temporal resolution of the original MICROBASE retrievals is 10s. The probabilistic PCA based ensemble means are of the same degree of magnitude as the original 0.5-hour ensemble means, but generally greater for thick clouds. The probabilistic PCA based standard deviation (STD, see Fig. 1d) is about 1/5 of the corresponding mean value in this case.

Using our developed UQ methodology, the average (min, max) values of the ice water path (IWP, unit: g/m^2) retrieved by MICROBASE are 25.4 (0.8, 119.4), respectively. IWP is derived consistently (i.e., integration over all the layers including the cloudless ones) for different approaches. Accordingly, cloudless layers are included when calculating 0.5-hour sample-mean of IWP derived from different approaches. The range is about a factor of 2 greater than the average numbers from 14 different retrievals shown in Table 2 of *Comstock et al.* [2007] (16.4 (0.076, 63.3)). We choose a large perturbation range (0.03–0.22 $(g/m^3)/dBZ$) of parameter "a" to cover various ice cloud conditions rather than the one-day case here as the goal is to quantify uncertainties in long-term ARM cloud retrievals. Despite the amplified parametric uncertainty, our IWP range falls into the individual retrieval range in *Comstock et al.* [2007]. It highlights the fact that propagating the uncertainties in the input data as well as the parameters through a single retrieval (i.e., MICROBASE) leads to the uncertainties in the output comparable to the differences amongst different retrievals, many of which are rooted from different theories/hypotheses and even based on different instruments. This implies that it might be possible to partly reconcile different algorithms by understanding the causes of the uncertainty in one of them. Through the variance-based sensitivity analysis performed by PSUADE, it is found that the parameter "a" is mainly responsible for the variability of the IWP retrieved by MICROBASE in this one-day case (see the Sobol's global sensitivity analysis section below for more details). Thus, the retrieval differences may be largely caused by how differently the parameter "a" is assumed (or implicit assumptions about the size, shape, and density of the target ice particles) by different algorithms.

Comparisons with independent observations (e.g., aircraft) provide another way to interpret our method. Figure 1e compares the IWP from the counterflow virtual impactor (CVI) (black line) [*Twohy et al.*, 1997] observation on the aircraft, original MICROBASE (red line), and our results (blue line). In general, the averages of in situ CVI measurements are greater than both retrievals and they agree within a factor of two, which has been revealed from a dozen of state-of-the-art retrievals comparisons (see Comstock et al., 2007 Fig. 5a). The differences between observations and retrievals are partly due to different sampling volumes, instrument uncertainties, sensitivities, and limitations [*Comstock et al.*, 2007]. Our probabilistic PCA based ensemble means of sample-means of retrieval products obtained by sampling perturbed MICROBASE are closer to the CVI probe measurements than the averages obtained from the original MICROBASE, which shows some encouraging signs of improving the retrieval results with our UQ method. This improvement is probably because our methodology parameterizes the input measurements based on the facts that (1) PCA extracts uncorrelated, independent random variables with orthogonal modes and the auto-correlation kernel is relatively more stable than instantaneous measurements within the 0.5-hour window; and (2) sample-mean is a smoother statistical variable and follows a normal distribution when the sampling size is large enough per CLT. In other words, targeting at the 0.5-hour observation window we replace the retrieval input of finite observations with normally distributed random fields. Statistically, it is thus more likely that the probabilistic PCA based ensemble means of the retrieved properties are closer to the reality than the ones using original algorithm.

The vertical bars in Fig. 1e are defined differently, but comparable. The CVI bars (black) represent the STDs of the 2-min IWP observations when the aircraft flew over the SGP site. The raw MICROBASE bars (red) depict the 0.5-hour STDs, while those of our results (blue) represent the STDs of sample-means within 0.5 hour window. Three types of bars overlap, which is consistent with *Comstock et al.* [2007]. Both methods generally show smaller uncertainties than the CVI observations, which likely reflects the large discrepancies in the sample volumes between the in situ observations and radar retrievals. However, to fully evaluate the proposed method and compare it with the original MICROBASE, the analysis needs to be expanded from the 1-day case to a longer time period that covers different seasons and cloud conditions.

It is worth noting that the probabilistic PCA based method includes a uniform perturbation from the parameter "a", whereas MICROBASE uses a constant value for the parameter "a". Nevertheless, targeting at the 0.5-hour time window, the uncertainties (standard deviations) of sample-means quantified by applying probabilistic PCA to the perturbed MICROBASE are generally smaller than those computed by the high-frequency original MICROBASE data. This highlights the fact that our probabilistic PCA based method estimates the uncertainty for the sample-mean of N observations within an interval chosen at model temporal resolution. The distribution of such statistic has a mean that equals to the interval population mean of the input data profiles and its variance equal to the variance of each instantaneous observation divided by N. Sample-mean is a good statistical estimator of the population mean of the input data profiles within the time window, where a "good" statistical estimator is defined as being efficient and unbiased in a statistical sense.

When keeping the parameter "a" as a constant, the probabilistic PCA based error bars are, as expected, much smaller than original MICROBASE (see Fig. 3). Great reduction in the probabilistic PCA based uncertainties when fixing parameter "a" (see Fig. 1e and Fig. 3) suggests that the parameter "a" is the main source of the uncertainty. In the following section, we will apply Sobol's sensitivity analysis to quantify the parametric uncertainty from the parameter "a", measurement uncertainty from radar profiles, and their possible interactions.

Figure 4 displays the box plot of IWC PDFs at 8 km (panel a) and the IWP PDFs (panel b). The retrievals exhibit larger spread in the probability distribution of both IWC and IWP for the optically thick clouds at 21:00–21:30 UTC. The IWP mean and STD at 21:00–21:30 UTC are $65.4\,\mathrm{g/m^2}$ and $28.7\,\mathrm{g/m^2}$, respectively; while its mean and STD at 22:00–22:30 UTC are $3.6\,\mathrm{g/m^2}$ and $1.6\,\mathrm{g/m^2}$, respectively. However, the IWP coefficients of variance defined as fraction of STD over mean are 0.4 for both 0.5-hour windows, whereas IWC at 8 km has slightly larger coefficient of variance at 22:00–22:30 UTC (0.5) than at 21:00–21:30 UTC (0.4). These results reinforce the needs of quantifying IWC uncertainties on different vertical layers.

4. Sobol's Sensitivity Analysis

Using PSUADE, Sobol's sensitivity analysis with bootstrapping [*Tong*, 2009] is implemented by resampling a response surface. Figures 5a–d show the results of Sobol's first and second order sensitivity analysis for IWP (left column) and IWC at 8 km (right column) at 22:00–22:30 UTC. Results for 21:00–21:30 UTC are similar and not shown. It is found that the parameter "a" is the major uncertainty source for both IWP and IWC with close to 1.0 Sobol's index (variance-based first-order sensitivity measure). This means that almost 100% of the output variance is caused by the variance in the parameter "a", whereas almost no variance of the output is caused by the variances in the radar reflectivity modes or interactions among them. Since the parameter "a" in the Z-IWC relationship is determined by the ice particle size, shape, and density, these characteristics need to be better described with more accurate cloud observations. This should be one emphasis area in future measurements.

In addition, the first mode of radar reflectivity (Z1) is the second largest uncertainty source (but much smaller than the parameter "a") within the time window 22:00–22:30 UTC. There are also small contributions from the interaction between the parameter "a" and Z1 (see Fig. 5d). The green points denote the uncertainties in Sobol's index due to statistical errors of resampling a response surface. These errors may cause Sobol's indices larger than one.

To separate out the measurement uncertainty (instrument noises) of radar profiles and their possible interactions from the parametric uncertainty, parallel results are shown for holding the parameter "a" as a constant in Figs. 6 and 7. Under this scenario, different radar reflectivity modes can be responsible for the IWP and IWC uncertainties at the same time (e.g., Fig. 6b vs. Fig. 7b). It should be noted that radar reflectivity modes with larger eigenvalues does not necessarily mean that they have more contributions on the variance of the IWP or IWC than other modes. For instance, in Fig. 7a (21:00–21:30 UTC), the second largest eigenvalue and the value for the corresponding radar reflectivity profile mode of IWC at 8km are 119 and -0.0222, respectively, while the third largest eigenvalue and the value for the corresponding radar reflectivity profile mode of IWC at 8km are 105 and -0.1030, respectively. Accordingly, the sensitivity of the second and the third radar reflectivity mode can be computed as $119 \times | - 0.0222| = 2.6418$ and $105 \times | - 0.1030| = 10.815$, respectively. It is found that the second radar reflectivity mode is less sensitive than the third one in this case. This means that there is no obvious correlation between eigenvalue and sensitivity for the extracted random variables using the EOF expansion. Similar rationales can be applied to study how various uncertainty sources contribute to the variability of IWP as well.

Therefore, this probabilistic PCA based sensitivity analysis is determined by both eigenvalues and corresponding spatial modes of the observed stochastic input profiles. As far as the sensitivity analysis is concerned, the contribution of variability of IWP due to radar reflectivity mode interactions is larger for the optically thin clouds observed at 22:00–22:30 UTC (Fig. 6d) than other periods such as the one observed at 21:00–21:30 UTC (Fig. 6c). Nevertheless, it is a different kind of variability analysis result for IWC at 8 km (see Figs. 7cd). Such quantitative knowledge with vertically resolved information about the relative contribution of individual error source to the output uncertainties provides valuable insights and clues to improve the both retrieval algorithm and measurements.

5. Conclusions and Discussions

Understanding and quantifying uncertainties in cloud retrieval is a subject of many earlier studies [*Comstock et al.*, 2007; *Turner et al.*, 2007; *Posselt et al.*, 2008; *Comstock et al.*, 2013; *Zhao et al.*, 2014]. Our contribution here is the development of a general, novel observation-based methodology to quantify the retrieval uncertainties for climate model evaluation. The EOF reduction of dimensions of random inputs enables our probabilistic PCA based approach to quantify vertically resolved uncertainty and conduct global sensitivity analysis. The UQ profiles with high vertical resolution are often more desirable for model evaluation as vertical structures of clouds are essential to many important topics such as radiative forcing and climate change [*Schneider*, 1972; *Schneider and Dickinson*, 1974; *Zelinka et al.*, 2012].

To reduce the dimensionality of random inputs, our method takes into account the correlation between vertical layers in the input data by adopting the EOF expansion. Moreover, by eliminating the unrealistic assumption that different layers are uncorrelated, the output uncertainty range becomes more accurate and reliable. Besides means and standard deviations, the proposed method also quantifies the full PDFs of retrieved quantities at each vertical layer. This observation-based PDF information can be used as *a priori* for the Bayesian approach [*McFarlane et al.*, 2002; *Posselt et al.*, 2008; *Shen et al.*, 2013] to avoid the so-called subjective uncertainty introduced by assuming *a priori* PDF (usually assumed to be uniform), and hence improve the results from Bayesian studies.

Besides propagating uncertainties in the input data and the parameters to retrieval outputs, this UQ approach has the capability of attributing the output uncertainties to individual error source, i.e., Sobol's global sensitivity analysis. This capacity is particularly useful when dealing with highly non-linear retrieval algorithms, as various error sources are more likely entangled.

Despite of the above advantages, this framework does not cover all the aspects of UQ analysis. For example, it cannot quantify systematic biases and the retrieval model structural uncertainty. The parameters of the retrieval algorithm may not be independent as assumed in this approach. For instance, parameters "a" and "b" in the Eq. (7) are dependent on each other [*Matrosov*, 1999]. In addition, some retrievals [*McFarlane et al.*, 2002; *Turner*, 2005; *Posselt et al.*, 2008] have already applied some uncertainty estimation approach, e.g. Bayesian calibration, and thus our approach may not be able to be directly applied to such algorithms.

The case study in this paper mainly demonstrates the capacities of this newly developed UQ methodology. We will expand the UQ analysis to long-term ARM observations to include different seasons and cloud types. Such comprehensive knowledge about retrieval uncertainties will facilitate the application of retrieval products in model evaluation and can be used to improve instruments, observation strategies as well as retrieval algorithms. We also plan to exploit the uncertainties of other retrieval algorithms. Using multi-retrieval and global model observations, we can further apply multi-model calibration technique to mitigate the uncertainty estimated by each retrieval algorithm.

Acknowledgments. The authors would like to thank the anonymous referees for their valuable comments that helped to clarify and improve the paper. We thank Michael Jensen, Matt Macduff, Laura Riihimaki, Chitra Sivaraman, and Timothy Shippert for helping the use of ARM MICROBASE, data, and computing facilities. Discussion with Charles Tong on applying PSUADE to uncertainty analysis of cloud retrievals is helpful.

The observational data were obtained from the ARM program sponsored by the U. S. Department of Energy, Office of Science, Office of Biological and Environmental Research, Environmental Sciences Division. Work at LLNL is supported by the DOE ARM and ASR programs and performed under the auspices of the U. S. Department of Energy by Lawrence Livermore National Laboratory under Contract No. DE-AC52-07NA27344. C. Zhao is partially supported by the Chinese program for New Century Excel-lent Talents in University and the Fundamental Research Funds for the Central Universities. This study is part of the ARM/ASR Quantification of Uncertainty in Cloud Retrieval (QUICR) focus group research activities. The data for the ice cloud case observed at the ARM SGP CF site can be accessed by linking to http://www.archive.arm.gov/armlogin/login.jsp.

Appendix A

Subtracting ensemble mean $\bar{y}(\mathbf{x})$ from each snapshot, we obtain a zero-mean $N \times n$ snapshot matrix

$$\mathbf{Y} = [y_1 - \bar{y}, y_2 - \bar{y}, \ldots, y_n - \bar{y}]. \tag{A1}$$

It should be noted that we take snapshots of relative error for radar reflectivity profiles and LWP, i.e., the snapshot matrix above is divided by $\bar{y}$, for which corresponding formulas can be derived similarly.

Without loss of generality, the following set of vectors

$$\Psi = \{\psi_1, \psi_2, \ldots, \psi_M\} \tag{A2}$$

of order $M \leq n$ provides an optimal representation of the ensemble data in a $M-$dimensional subspace by minimizing the averaged projection error

$$\min_{\{\psi_1,\psi_2,\ldots,\psi_M\}} \frac{1}{n}\sum_{i=1}^{n} \left\|(y_i - \bar{y}) - \Pi_{\Psi,M}(y_i - \bar{y})\right\|^2$$
$$\text{s.t. } \langle \psi_i, \psi_j \rangle = \delta_{ij} = \begin{cases} 1 & i = j \\ 0 & i \neq j \end{cases}, \tag{A3}$$

where $\langle \cdot, \cdot \rangle$ represents an inner product, and $\Pi_{\Psi,M} = \sum_{i=1}^{M} \langle y_i - \bar{y}, \psi_i \rangle \psi_i$ is the projection operator onto the M-dimensional space spanned by Ψ.

To compute the EOFs or the modes of PCA $\psi_i \in \mathbb{R}^N$ satisfying Eq. (A3), one solves an $N-$dimensional eigenvalue problem

$$\mathbf{A}\psi_i = \lambda_i \psi_i, \tag{A4}$$

where $\mathbf{A} = \mathbf{Y}\mathbf{Y}^{\mathbf{T}}$ is the spatial correlation matrix.

Since in practice the number of snapshots is much less than the the state dimension, $n << N$, an efficient way to compute the reduced basis is to introduce a $n-$dimensional matrix $\mathbf{K} = \mathbf{Y^T Y}$ and compute the eigenvalues $\lambda_1 \geq \lambda_2 \geq \ldots \geq \lambda_n \geq 0$ of $\mathbf{K}$ with its corresponding eigenvectors $\phi_1, \ldots, \phi_n$. The corresponding EOF or modes of PCA are thus obtained by

$$\psi_i = \frac{1}{\sqrt{\lambda_i}} \mathbf{Y} \phi_i, \quad i = 1, \ldots, M, \tag{A5}$$

where $\langle \psi_i, \psi_j \rangle = \delta_{ij}$.

One can define a relative information content to choose a low-dimensional basis of size $M << n$ by neglecting modes corresponding to the small eigenvalues. We define

$$I\left(m\right) = \frac{\sum_{i=1}^{i=m} \lambda_i}{\sum_{i=1}^{i=n} \lambda_i} \tag{A6}$$

and choose M such that $M = \arg\min \left\{ I\left(m\right) : I\left(m\right) > \gamma \right\}$, where $0 \leq \gamma \leq 1$ is the percentage of total information retained in the reduced space and the tolerance γ must be chosen to be close unity in order to capture most of the energy of the snapshots basis. A fast algorithm for eigenvalue calculation using a transposed matrix can be referenced [*Shen et al.*, 2014].

Therefore, for each one observation y_i, it can be expanded in terms of M numbers of EOFs or modes of PCA written as

$$y_i = \bar{y} + \sum_{i=1}^{M} \psi_i \sqrt{\frac{\lambda_i}{n}} V_i, \tag{A7}$$

where modal coefficients V_i computed by

$$V_i = \psi_i^{\mathbf{T}} y_i \sqrt{\frac{n}{\lambda_i}}, \tag{A8}$$

such that $\langle V_i, V_j \rangle = \delta_{ij}$.

Since mean is subtracted from each snapshots, it can be shown that $\frac{1}{n}\sum_{j=1}^{n}(V_{ij}) = 0$, where V_{ij} corresponds to the observation $y_j - \bar{y}$ projected onto the mode ψ_i.

As a result, $Y(\mathbf{x}, t, \theta)$ can be approximated by EOF expansion to the order of M as

$$Y(\mathbf{x}, t, \theta) = \bar{y} + \sum_{i=1}^{M} \psi_i \sqrt{\frac{\lambda_i}{n}} \xi_i, \tag{A9}$$

such that $E(\xi_i) = 0$ and $E(\xi_i \xi_j) = \delta_{ij}$, $i = 1, \ldots, M$, and ξ_i follows some unknown distribution.

Appendix B

Let $w = [w_1, w_2, \ldots, w_N]^{\mathbf{T}}$ be a temporally independent Gaussian noise injected into each one of the observation y_i. Therefore, w follows a multivariate normal distribution defined as $w \sim \mathcal{N}(0, \sigma_0^2 \mathbf{I}_N)$, where $\mathbf{I}_N$ is a $N \times N$ identity matrix. Since Ψ is an orthogonal transformation, Ψw follows the same distribution as w, i.e., $\Psi w \sim \mathcal{N}(0, \sigma_0^2 \mathbf{I}_N)$. Therefore, without loss of generality, adding Ψw to the Equation (A9) and truncating it to the order of M, we obtain that

$$\begin{aligned} Y'(\mathbf{x}, t, \theta) &= Y(\mathbf{x}, t, \theta) + \Psi w \\ &= \bar{y} + \sum_{i=1}^{M} \psi_i \sqrt{\frac{\lambda_i}{n}} \xi_i + \sum_{i=1}^{M} \psi_i w_i \\ &= \bar{y} + \sum_{i=1}^{M} \psi_i \sqrt{\frac{\lambda_i}{n}} \left(\xi_i + \frac{w_i}{\sqrt{\frac{\lambda_i}{n}}} \right), \end{aligned} \tag{B1}$$

where $Y'(\mathbf{x}, t, \theta)$ is a stochastic process representing noisy observations, w_i is the i-th component of the truncated random vector Ψw.

Let ζ_i be $\zeta_i = \xi_i + \frac{w_i}{\sqrt{\frac{\lambda_i}{n}}}$, we obtain

$$Y'(\mathbf{x}, t, \theta) = \bar{y} + \sum_{i=1}^{M} \psi_i \sqrt{\frac{\lambda_i}{n}} \zeta_i, \tag{B2}$$

where $E(\zeta_i) = 0$ and $Var(\zeta_i) = \sqrt{1 + \left(\frac{\sigma_0}{\sqrt{\frac{\lambda_i}{n}}} \right)^2}$.

Taking average on both sides of the Eq. (B2) above, it can be rewritten as

$$\overline{Y'}(\mathbf{x}, t, \theta) = \bar{y} + \sum_{i=1}^{M} \psi_i \sqrt{\frac{\lambda_i}{n}} \overline{\zeta_i}. \tag{B3}$$

Finally, based on CLT [*Cramér*, 1946; *Gnedenko et al.*, 1954] and considering the truncation error, we have

$$\overline{Y'}\left(\mathbf{x},t,\theta\right)=\bar{y}+\sum_{i=1}^{M}\psi_i\sqrt{\frac{\lambda_i}{n}}\sqrt{1+\left(\frac{\sigma_0}{\sqrt{\frac{\lambda_i}{n}}}\right)^2}\frac{z_i}{\sqrt{n}}+error\left(\mathbf{x},t,\theta\right), \tag{B4}$$

where $z_i \sim \mathcal{N}\left(0,1\right)$, and the $error\left(\mathbf{x},t,\theta\right)$ represents the truncation error incurred in the expansion above, which can be estimated following [*Shen et al.*, 2004, 2014].

References

Chen, X., B. M. Ng, Y. Sun, and C. H. Tong (2013), A computational method for simulating subsurface flow and reactive transport in heterogeneous porous media embedded with flexible uncertainty quantification, *Water Resour. Res.*, *49*, 1–16.

Comstock, J. M., A. Protat, S. A. McFarlane, J. Delanoë, and M. Deng (2013), Assessment of uncertainty in cloud radiative effects and heating rates through retrieval algorithm differences: Analysis using 3 years of arm data at darwin, australia, *J. Geophys. Res.*, *118*, 4549–4571.

Comstock, N. M., R. D. Entremont, D. Deslover, and C. G. Mace (2007), An intercomparison of microphysical retrieval algorithms for upper tropospheric ice clouds, *Bull. Am. Meteorol. Soc*, *88*, 191–204.

Cramér, H. (1946), *Mathematical methods of statistics*, *Princeton mathematical series*, vol. 9, xvi + 575 pp., Princeton University Press.

Dunn, M., K. L. Johnson, and M. P. Jensen (2011), The microbase value-added product: A baseline retrieval of cloud microphysical properties, *Tech. rep.*, Dept. of Energy, Washington, D. C.

Gnedenko, B. V., A. N. Kolmogorov, K. L. Chung, and J. L. Doob (1954), *Limit distributions for sums of independent random variables*, Addison-Wesley Publishing Company, Inc., Cambridge, Mass., trans. and annotated by K. L. Chung.

Hotelling, H. (1933), Analysis of a complex of statistical variables into principal components, *J. Educ. Psychol.*, *24*(1), 417–441, 498–520.

Huang, D., C. Zhao, M. Dunn, X. Dong, G. Mace, M. P. Jensen, S. Xie, and Y. Liu (2012), An intercomparison of radar-based liquid cloud microphysics retrievals and implication for model evaluation studies, *Atmos. Meas. Tech.*, *5*, 1409–1424, doi:10.5194/amt-5-1409-2012.

Kosambi, D. D. (1943), Statistics in function space, *J. Indian Math. Soc.*, *7*(1), 559–572.

Kuhunen, K. (1947), Uber lineare methoden in der wahrscheinlichkeitsrechnung, *Ann. Acad. Sci. Fenn.*, *37*, 1–79.

Liu, C. L., and A. J. Illingworth (2000), Toward more accurate retrievals of ice water content from radar measurements of clouds, *J. Appl. Meteorol.*, *39*(7), 1130–1146.

Loéve, M. (1945), Fonctions aleatoires de second ordre, *C. R. Acad. Sci*, *220*(469).

Määttä, A., M. Laine, J. Tamminen, and J. P. Veefkind (2014), Quantification of uncertainty in aerosol optical thickness retrieval arising from aerosol microphysical model and other sources, applied to ozone monitoring instrument (omi) measurements, *Atmos. Meas. Tech.*, *7*, 1185–1199.

Matrosov, S. Y. (1999), Retrievals of vertical profiles of ice cloud microphysics from radar and IR measurements using tuned regressions between reflectivity and cloud parameters, *J. Geophys. Res.*, *104*(D14), 16,741–16,753, doi:10.1029/1999JD900244.

McFarlane, S. A., K. F. Evans, and A. S. Ackerman (2002), A bayesian algorithm for the retrieval of liquid water cloud properties from microwave radiometer and millimeter radar data, *J. Geophys. Res.*, *107*(D16), 4317, doi:10.1029/2001JD001011.

McKay, M. C., R. Beckman, and W. Conover (1979), A comparison of three methods for selecting values of input variables in the analysis of output from a computer code, *Technometrics*, *21*(2), 239–245.

Pearson, K. (1901), On lines and planes of closest fit to systems of points in space, *Philos. Mag.*, *2*(6), 559–572.

Posselt, D. J., T. S. L'Ecuyer, and G. L. Stephens (2008), Exploring the error characteristics of thin ice cloud property retrievals using a Markov chain Monte Carlo algorithm, *J. Geophys. Res.*, *113*(D24), D24,206, doi:10.1029/2008JD010832.

Schneider, S. H. (1972), Cloudiness as a global climatic feedback mechanism: the effects on the radiation balance and surface temperature of variations in cloudiness, *J. Atmos. Sci.*, *29*(8), 1413–1422.

Schneider, S. H., and R. E. Dickinson (1974), Climate modeling, *Rev. Geophys.*, *12*(3), 447–493, doi:10.1029/RG012i003p00447.

Shen, S. S. P., A. N. Basist, G. Li, C. Williams, and T. R. Karl (2004), Multivariate regression reconstruction and its sampling error for the quasi-global annual precipitation from 1900 to 2011, *Environmetrics*, *15*, 233–249.

Shen, S. S. P., V. M. Velado, R. C. J. Somerville, and G. J. Kooperman (2013), Probabilistic assessment of cloud fraction using bayesian blending of independent datasets: feasibility study of a new method, *J. Geophys. Res.*, *118*(10), 4644–4656, doi:10.1002/jgrd.50408.

Shen, S. S. P., N. Tafolla, T. M. Smith, and P. A. Arkin (2014), Multivariate regression reconstruction and its sampling error for the quasi-global annual precipitation from 1900 to 2011, *J. Atmos. Sci.*, *71*, 3250–3268.

Sirovich, L., J. L. Lumley, and G. Berkooz (1987), Turbulence and the dynamics of coherent structures, part iii: dynamics and scaling, *Q. Appl. Math.*, *45*(3), 583–590.

Sobol', I. (1993), Sensitivity estimates for nonlinear mathematical models, *Math. Modeling Comput. Experiment*, *1*(4), 407–414.

Storch, H. V., and F. W. Zwiers (2002), *Statistical Analysis in Climate Research*, Cambridge University Press.

Tong, C. (2009), *PSUADE User's Manual (Version 1.2.0)*, Lawrence Livermore National Laboratory, lLNL-SM-407882.

Turner, D. D. (2005), Arctic mixed-phase cloud properties from aeri lidar observations: algorithm and results from sheba, *J. Appl. Meteor.*, *44*(4), 427–444, doi: 10.1175/JAM2208.1.

Turner, D. D., S. A. Clough, J. C. Liljegren, E. E. Clothiaux, K. Cady-Pereira, and K. L. Gaustad (2007), Retrieving liquid water path and precipitable water vapor from atmospheric radiation measurement (arm) microwave radiometers, *IEEE Trans. Geosci. Remote Sens.*, *45*(11), 3680–3690.

Twohy, C. H., A. J. Schanot, and W. A. Cooper (1997), Measurement of condensed water content in liquid and ice clouds using an airborne counterflow virtual impactor, *J. Atmos. Oceanic Technol.*, *14*, 197–202.

Wilks, D. S. (2011), *Statistical Methods in the Atmospheric Sciences*, vol. 100, third edition ed., Academic Press.

Xie, S., M. Zhang, and other coauthors (2005), Simulations of midlatitude frontal clouds by scms and csrms during the arm march 2000 cloud iop, *J. Geophys. Res.*, *110*(D15S03), doi:10.1029/2004JD005119.

Xie, S., A. Protat, and other coauthors (2011), Focus group proposal whitepaper: Asr quantification of uncertainty in cloud retrievals (quicr) focus group, *Tech. rep.*, DOE cloud retrievals focus group.

Xu, K. M., M. Zhang, and other coauthors (2005), Modeling springtime shallow frontal clouds with cloud-resolving and single-column models, *J. Geophys. Res.*, *110*(D15S04), doi:10.1029/2004JD005153.

Zelinka, M. D., S. A. Klein, and D. L. Hartmann (2012), Computing and partitioning cloud feedbacks using cloud property histograms. part II: Attribution to changes in cloud amount, altitude, and optical depth, *J. Climate*, *25*(11), 3736–3754, doi:10.1175/JCLI-D-11-00249.1.

Zhao, C., S. Xie, and K. A. Stephen (2012), Toward understanding of differences in current cloud retrievals of arm ground-based measurements, *J. Geophys. Res.*, *117*(D10), 1–21.

Zhao, C., S. Xie, X. Chen, M. P. Jensen, and M. Dunn (2014), Quantifying uncertainties of cloud microphysical property retrievals with a perturbation method, *J. Geophys. Res.*, *119*, 1–11.

Figure 1. Height-time plots at SGP CF site on March 9, 2000 for (a) MMCR reflectivity (dBZ); (b) 0.5-hour averages of IWC (g/m^3) from raw MICROBASE; (c) 0.5-hour ensemble means (ensemble size=1000), and (d) standard deviations (STDs, σ) of IWC from probabilistic PCA based method; (e) comparison of 0.5-hour IWP (g/m^2) from probabilistic PCA based method (blue), raw MICROBASE (red), and 2-min in-situ CVI measurements (black) as aircraft passed over the SGP CF site. Dashed lines connect the means, and error bars represent $\pm 1\sigma$.

Figure 2. Height-time plots at SGP CF site on March 9, 2000 for the leading four MMCR reflectivity (dBZ) profiles modes, marked with corresponding eigenvalues and weighting percentage to capture the energy of snapshots of radar reflectivity profiles within each time window.

Figure 3. Comparison of 0.5-hour IWP (g/m^2) from probabilistic PCA based method (blue) when keeping a as a constant, raw MICROBASE (red), and 2-min in-situ CVI measurements (black) as aircraft passed over the SGP CF site. Dashed lines connect the means, and error bars represent $\pm 1\sigma$.

Figure 4. Probability density functions derived from probabilistic PCA based method of (a) IWC (g/m^3) at 8 km, 19:00–22:30 shown as box plot (red lines: median; lower/upper blue box lines: lower/upper quartiles; whiskers show the extent of the data); (b) IWP (g/m^2) at 21:00–21:30 UTC (green) and 22:00–22:30 UTC (black) on March 9, 2000.

Figure 5. Sobol's first-order index of (a) IWP and (b) IWC at 8 km, and Sobol's first and second order (i.e., the sum of two different first order index and their joint index, Note that the diagonal and sub-diagonal numbers are not shown by definition.) index of (c) IWP and (d) IWC at 8 km. All the results are for March 9, 2000 22:00–22:30 UTC.

Figure 6. Sobol's first-order index of IWP for (a) 2100–21:30 UTC and (b) 22:00–22:30 UTC, and Sobol's first and second order (i.e., the sum of two different first order index and their joint index, Note that the diagonal and sub-diagonal numbers are not shown by definition.) index of IWP for (c) 2100–21:30 UTC and (d) 22:00–22:30 UTC. All the results are for March 9, 2000.

Figure 7. Sobol's first-order index of IWC at 8 km for (a) 2100–21:30 UTC and (b) 22:00–22:30 UTC, and Sobol's first and second order (i.e., the sum of two different first order index and their joint index, Note that the diagonal and sub-diagonal numbers are not shown by definition.) index of IWP for (c) 2100–21:30 UTC and (d) 22:00–22:30 UTC. All the results are for March 9, 2000.

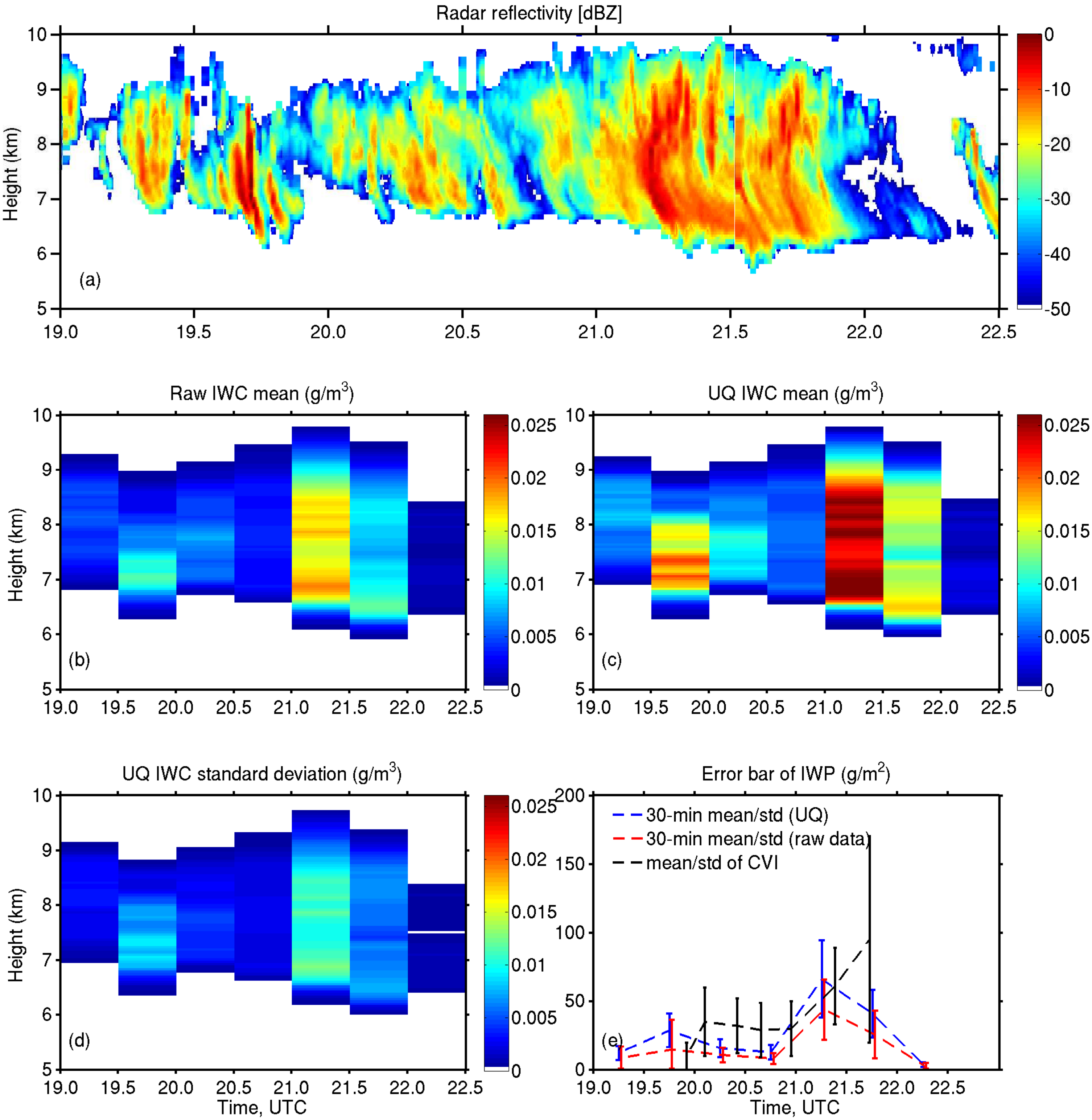
Radar reflectivity [dBZ]
Height (km)
(a)
Raw IWC mean (g/m3)
(b)
UQ IWC mean (g/m3)
(c)
UQ IWC standard deviation (g/m3)
(d)
Time, UTC
Error bar of IWP (g/m2)
30-min mean/std (UQ)
30-min mean/std (raw data)
mean/std of CVI
(e)

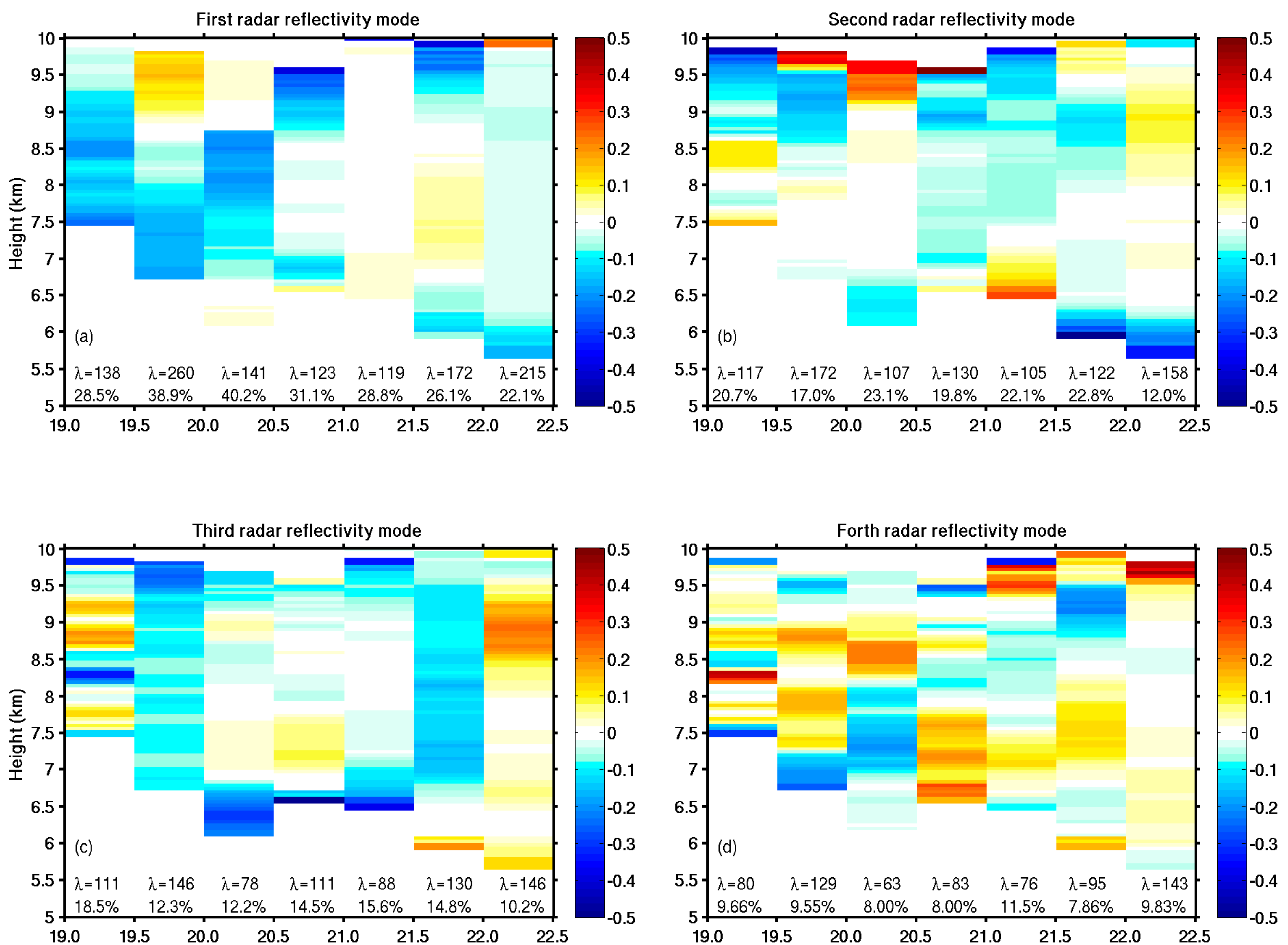

First radar reflectivity mode
Second radar reflectivity mode
Third radar reflectivity mode
Forth radar reflectivity mode
Height (km)
(a)
λ=138 28.5%
λ=260 38.9%
λ=141 40.2%
λ=123 31.1%
λ=119 28.8%
λ=172 26.1%
λ=215 22.1%
(b)
λ=117 20.7%
λ=172 17.0%
λ=107 23.1%
λ=130 19.8%
λ=105 22.1%
λ=122 22.8%
λ=158 12.0%
(c)
λ=111 18.5%
λ=146 12.3%
λ=78 12.2%
λ=111 14.5%
λ=88 15.6%
λ=130 14.8%
λ=146 10.2%
(d)
λ=80 9.66%
λ=129 9.55%
λ=63 8.00%
λ=83 8.00%
λ=76 11.5%
λ=95 7.86%
λ=143 9.83%
19.0 19.5 20.0 20.5 21.0 21.5 22.0 22.5
5 5.5 6 6.5 7 7.5 8 8.5 9 9.5 10
-0.5 -0.4 -0.3 -0.2 -0.1 0 0.1 0.2 0.3 0.4 0.5

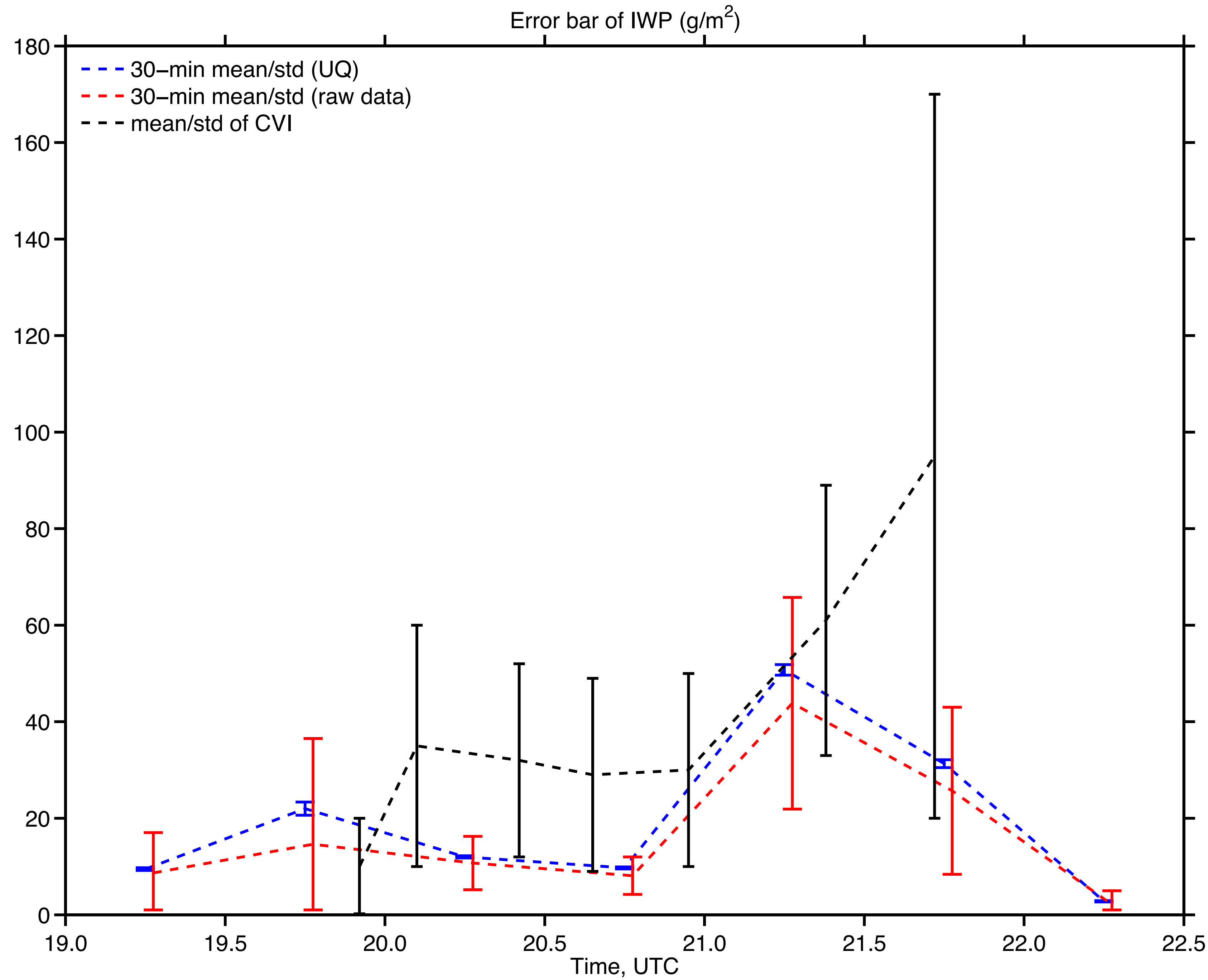
Error bar of IWP (g/m2)
30–min mean/std (UQ)
30–min mean/std (raw data)
mean/std of CVI
0
20
40
60
80
100
120
140
160
180
19.0
19.5
20.0
20.5
21.0
21.5
22.0
22.5
Time, UTC

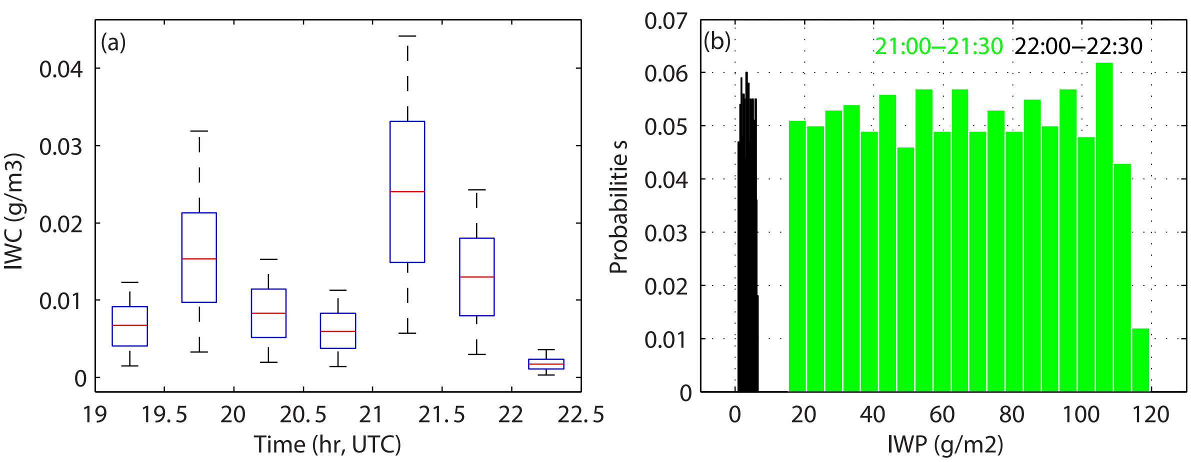
(a)
IWC (g/m3)
0.04
0.03
0.02
0.01
0
19
19.5
20
20.5
21
21.5
22
22.5
Time (hr, UTC)
(b)
21:00–21:30
22:00–22:30
Probabilities
0.07
0.06
0.05
0.04
0.03
0.02
0.01
0
0
20
40
60
80
100
120
IWP (g/m2)

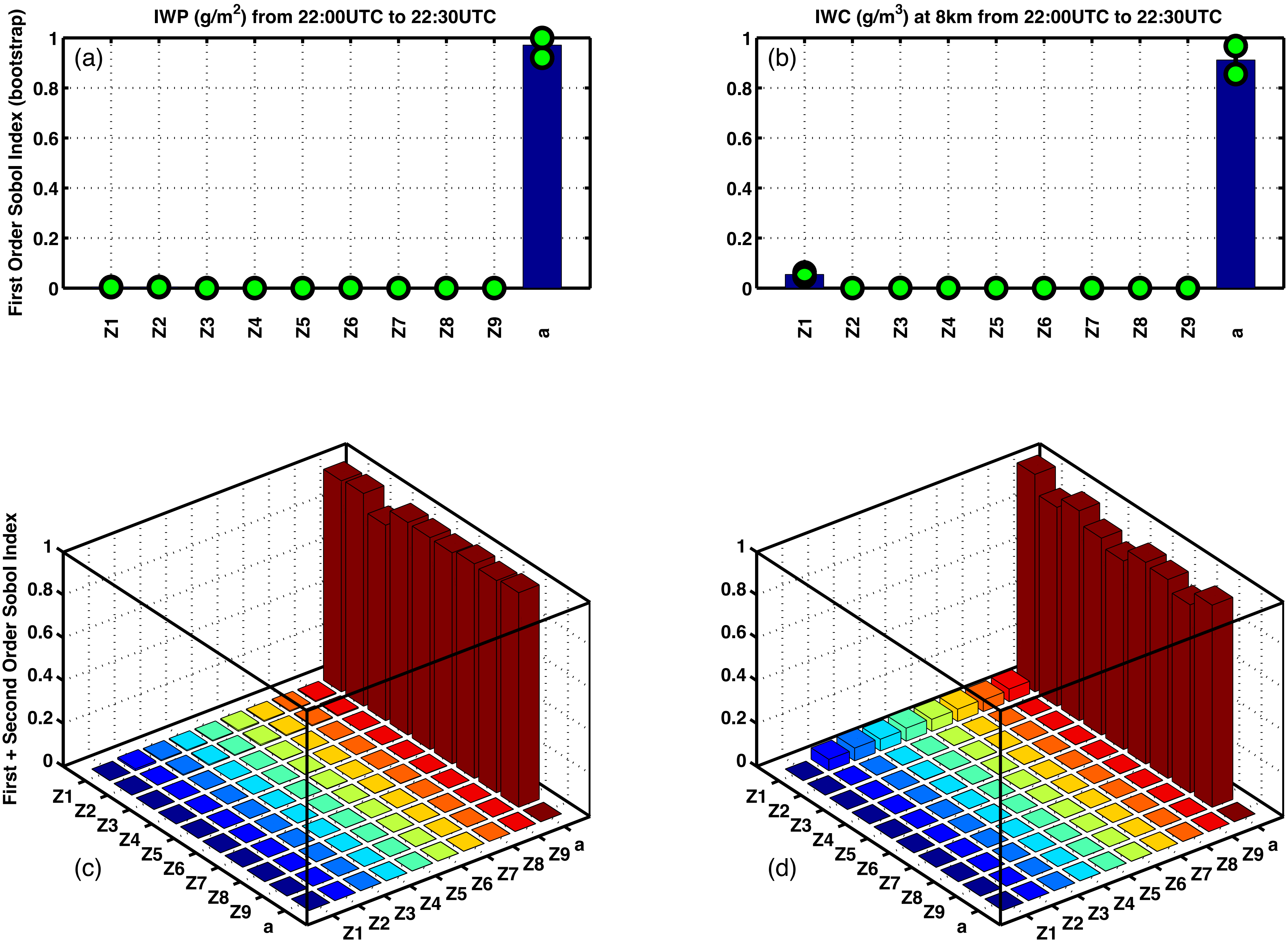

IWP (g/m^2) from 22:00UTC to 22:30UTC
IWC (g/m^3) at 8km from 22:00UTC to 22:30UTC
First Order Sobol Index (bootstrap)
First + Second Order Sobol Index
(a)
(b)
(c)
(d)
0
0.2
0.4
0.6
0.8
1
Z1
Z2
Z3
Z4
Z5
Z6
Z7
Z8
Z9
a

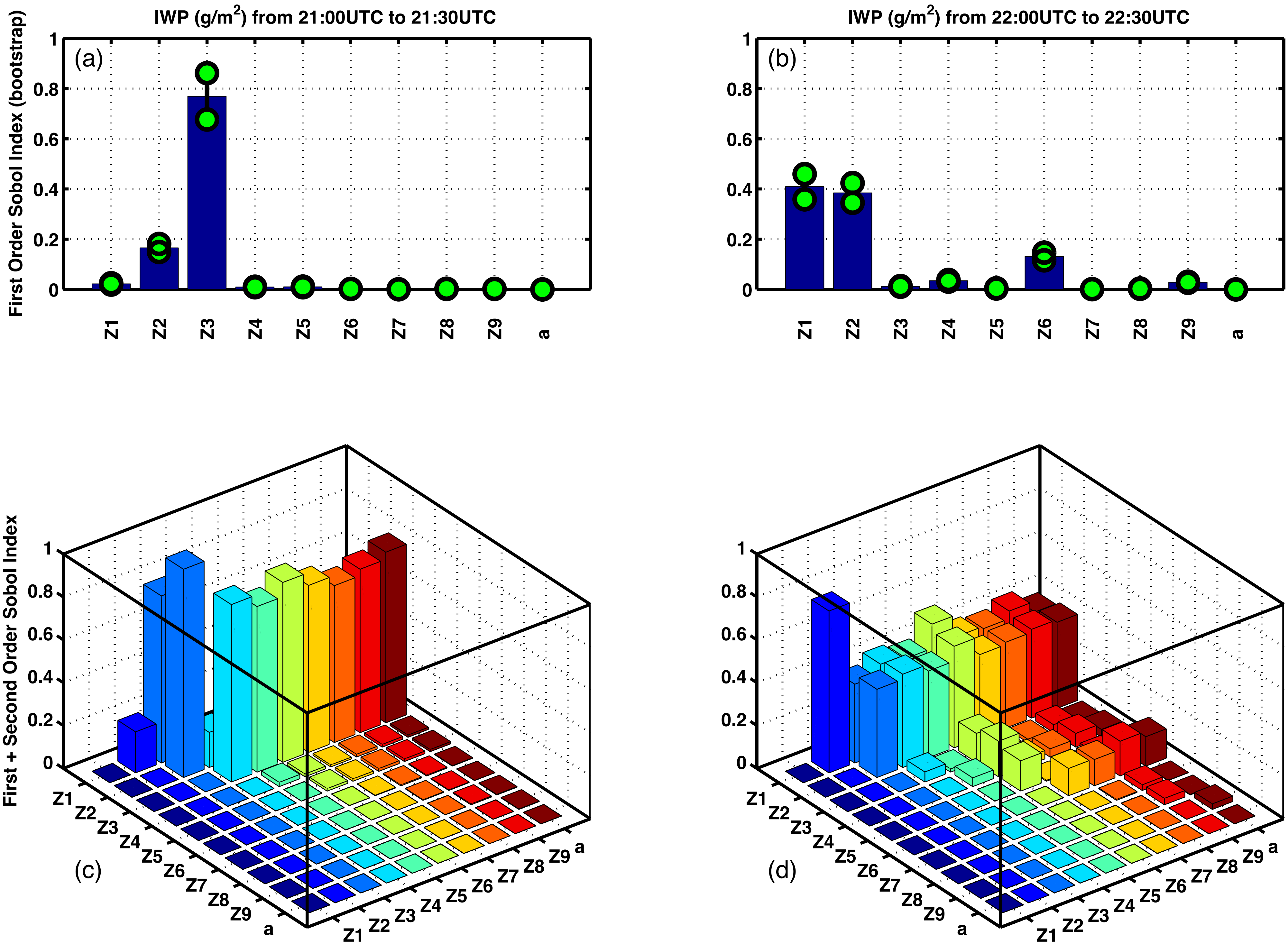
IWP (g/m^2) from 21:00UTC to 21:30UTC
IWP (g/m^2) from 22:00UTC to 22:30UTC
First Order Sobol Index (bootstrap)
First + Second Order Sobol Index
(a)
(b)
(c)
(d)
Z1 Z2 Z3 Z4 Z5 Z6 Z7 Z8 Z9 a
0 0.2 0.4 0.6 0.8 1

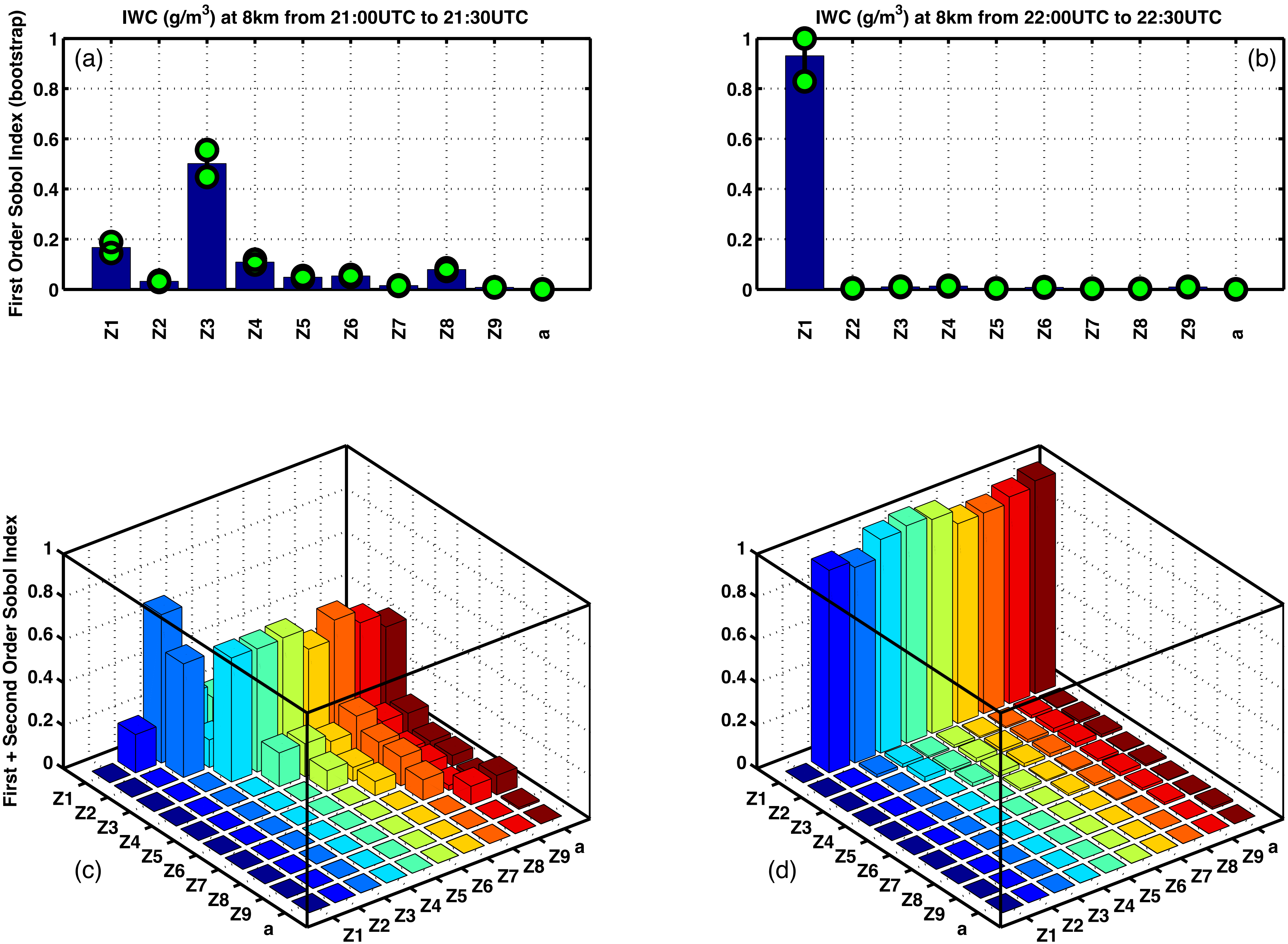
IWC (g/m3) at 8km from 21:00UTC to 21:30UTC
IWC (g/m3) at 8km from 22:00UTC to 22:30UTC
First Order Sobol Index (bootstrap)
(a)
(b)
First + Second Order Sobol Index
(c)
(d)
Z1
Z2
Z3
Z4
Z5
Z6
Z7
Z8
Z9
a
0
0.2
0.4
0.6
0.8
1